

DRCT: Saving Image Super-Resolution away from Information Bottleneck

Chih-Chung Hsu, Chia-Ming Lee, Yi-Shiuan Chou
 Institute of Data Science, National Cheng Kung University

cchsu@gs.ncku.edu.tw, zuw408421476@gmail.com, nelly910421@gmail.com

Abstract

In recent years, Vision Transformer-based applications to low-level vision tasks have achieved widespread success. Unlike CNN-based models, Transformers are more adept at capturing long-range dependencies, enabling the reconstruction of images utilizing information from non-local areas. In the domain of super-resolution, Swin-transformer-based approaches have become mainstream due to their capacity to capture global spatial information and their shifting-window attention mechanism that facilitates the interchange of information between different windows. Many researchers have enhanced image quality and network efficiency by expanding the receptive field or designing complex networks, yielding commendable results. However, we observed that spatial information tends to diminish during the forward propagation process due to increased depth, leading to a loss of spatial information and, consequently, limiting the model's potential. To address this, we propose the Dense-residual-connected Transformer (DRCT), aimed at mitigating the loss of spatial information through dense-residual connections between layers, thereby unleashing the model's potential and enhancing performance. Experiment results indicate that our approach is not only straightforward but also achieves remarkable efficiency, surpassing state-of-the-art methods and performing commendably at NTIRE2024.

1. Introduction

The task of Single Image Super-Resolution (SISR) is aimed at reconstructing a high-quality image from its low-resolution version. This quest for effective and skilled super-resolution algorithms has become a focal point of research within the field of computer vision, owing to its wide range of applications.

Following the foundational studies, CNN-based strategies [8, 10, 25, 31, 32, 56] have predominantly governed the super-resolution domain for an extended period. These strategies largely leverage techniques such as residual learning [19, 26, 38, 43, 53], or channel attention [46, 52] for de-

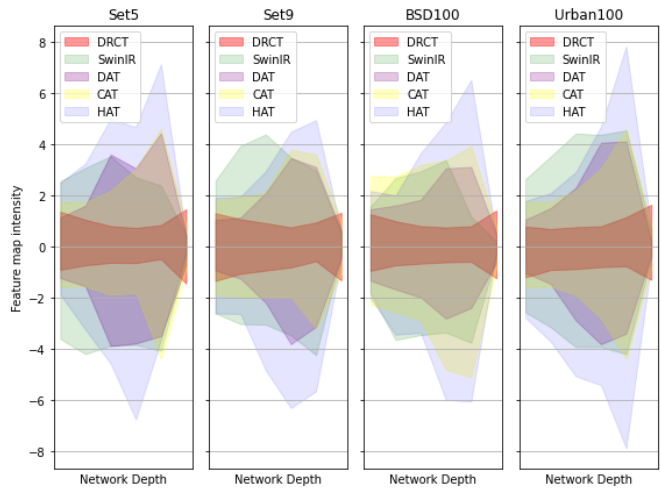


Figure 1. The feature map intensity on various benchmark datasets. We observed that feature map intensities decrease sharply at deeper network levels, indicating potential information loss. We propose DRCT, stabilizes this by enhancing receptive fields and adding dense-connections within residual blocks to mitigate information bottlenecks, thereby improving performance with a simpler model design.

veloping network architectures, significantly propelling the progress of super-resolution models forward.

CNN-based networks have achieved notable success in terms of performance. However, their inherent limitations stem from the parameter-dependent scaling of the receptive field and the local nature of convolutional interactions, which are independent of content. These characteristics limit CNNs' ability to effectively model long-range dependencies.

To overcome the limitations associated with CNN-based networks, researchers have introduced Transformer-based SISR networks that leverage the capability to model long-range dependencies, thereby enhancing SISR performance. Notable examples include IPT [3] and EDT [22], which utilize pre-training on the ImageNet [9] dataset to fully leverage Transformer capabilities for superior SISR results. SwinIR [24], inspired by the Swin-transformer [27] archi-

ture, marks a significant advancement in SISR performance.

This approach significantly enhances capabilities beyond those of traditional CNN-based models across various benchmarks. Following SwinIR’s success, several works [5, 7, 21, 24, 50, 51, 57, 58] have built upon its framework. These subsequent studies leverage Transformers to innovate diverse network architectures specifically for super-resolution tasks, showcasing the evolving landscape of SISR technology through the exploration of new architectural innovations and techniques.

While using HAT and SwinIR for inference across various datasets, we observed a common phenomenon: the intensity distribution of the feature maps undergoes more substantial changes as the network depth increases. This indicates the spatial information and attention intensity learned by the model. However, there’s often a sharp decrease towards the end of the network, shrinking to a smaller range. This intriguing pattern suggests that such abrupt changes might be accompanied by a loss of information, indicating the presence of an information bottleneck.

Inspired by a series of works by Wang *et al.*, such as the YOLO-family [39, 42], CSPNet [40], and ELAN [41], we consider that network architectures based on SwinIR, despite significantly enlarging the receptive field through shift-window attention to address the issue of insufficient receptive fields in CNNs, are prone to gradient bottlenecks due to the loss of spatial information as network depth increases. This implicitly constrains the model’s performance.

To address the issue of spatial information loss due to an increased number of network layers, we introduce the Dense-residual-connected Transformer (DRCT), designed to stabilize the forward-propagation process and prevent information bottlenecks. This is achieved by the proposed Swin-Dense-Residual-Connected Block (SDRCB), which incorporates Swin Transformer Layers and transition layers into each Residual Deep Feature Extraction group (RD-FEG). Consequently, this approach enhances the receptive field with fewer parameters and a simplified model structure, thereby resulting in improved performance.

2. Related works

2.1. Vision Transformer-based Super-resolution

IPT [3], a versatile model utilizing the Transformer encoder-decoder architecture, has shown efficacy in super-resolution, along with denoising and deraining tasks. SwinIR [24], building on the Swin Transformer [27] encoder, employs self-attention within local windows during feature extraction, resulting in superior performance. UFormer [44] introduces an innovative local-enhancement window Transformer block, greatly reducing computational

demands for processing high-resolution features. Furthermore, it introduces a learnable multi-scale restoration modulator within the decoder to enhance the model’s ability to detect both local and global patterns necessary for image restoration. ART [58] incorporates an attention retractable module to expand its receptive field, thereby enhancing SISR performance. CAT [6] leverages rectangle-window self-attention for feature aggregation, achieving a broader receptive field. It also integrates a locality complementary module to effectively merge global and local information, improving image restoration outcomes. HAT [5] integrates channel attention with window-based self-attention, leveraging both global information and precise local fitting abilities. Additionally, it introduces an overlapping cross-attention module, specifically designed to improve the aggregation of information across different windows, thereby enhancing feature interaction and setting new benchmarks in the field.

2.2. Auxiliary Supervision and Feature Fusion

Auxiliary Supervision. Deep supervision is a commonly used auxiliary supervision method [20, 33] that involves training by adding prediction layers at the intermediate levels of the model [39–41]. This approach is particularly prevalent in architectures based on Transformers that incorporate multi-layer decoders. Another popular auxiliary supervision technique involves guiding the feature maps produced by the intermediate layers with relevant metadata to ensure they possess attributes beneficial to the target task [14, 15, 18, 43, 53]. Choosing the appropriate auxiliary supervision mechanism can accelerate the model’s convergence speed, while also enhancing its robustness and performance.

Feature Fusion. Various studies have explored the integration of features across different dimensions in multiple visual tasks [26, 47] to enhance performance. In CNNs, attention mechanisms have been applied to both spatial and channel dimensions to improve feature representation; examples of which include RTCS [16] and SwinFusion [28]. In ViT [11], spatial self-attention is used to model the long-range dependencies between pixels. Additionally, some researchers have investigated the incorporation of channel attention within Transformers [4, 55] to effectively amalgamate spatial and channel information. This integration significantly enhances the modeling capabilities of Transformers.

3. Problem Statement

3.1. Information Bottleneck Principle

According to the information bottleneck principle [37], the given data X may cause information loss when going through consecutive layers. It may lead to gradient vanish

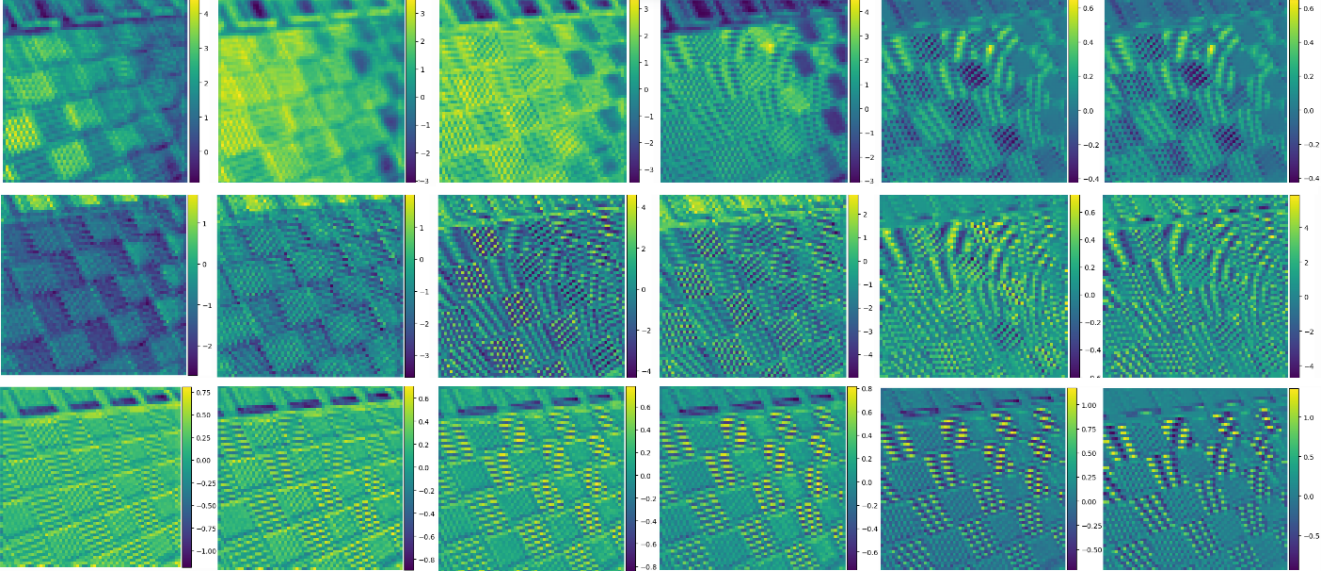


Figure 2. The feature map visualization displays, from top to bottom, SwinIR [24], HAT [5], and DRCT, with positions further to the right representing deeper layers within the network. For both SwinIR and HAT, the intensity of the feature maps is significant in the shallower layers but diminishes towards the network’s end. We consider this phenomenon may imply the loss of spatial information, leading to the limitation and information bottleneck with SISR tasks.

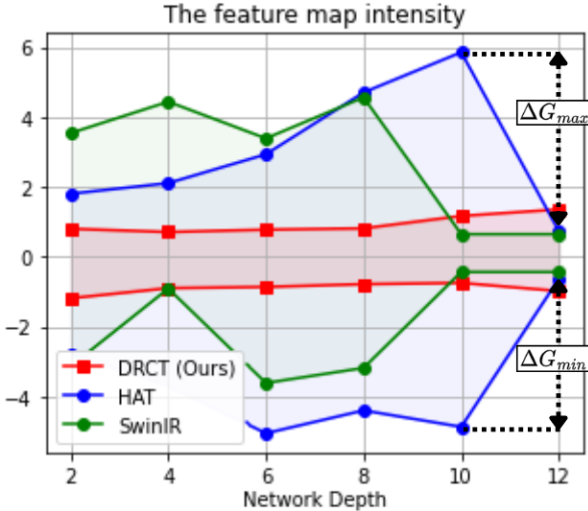


Figure 3. The G-index we propose is calculated by summing the absolute values of ΔG_{min} and ΔG_{max} , where ΔG represents the change in feature map intensity between two consecutive layers. This change is measured by the difference in intensity levels, capturing both the minimum and maximum shifts across layers.

when back-propagation for fitting network parameters and predicting Y , as shown in the equation below:

$$I(X, X) \geq I(Y, X) \geq I(Y, f_\theta(X)) \geq I(Y, g_\phi(f_\theta(X))) \geq \dots \geq I(Y, \hat{Y}) \quad (1)$$

where I indicates mutual information, f and g are transformation functions, and θ and ϕ are parameters of f and g ,

respectively.

In deep neural networks, $f_\theta(\cdot)$ and $g_\phi(\cdot)$ respectively represent the two consecutive layers in neural network. From equation 1, we can predict that as the number of network layer becomes deeper, the original data will be more likely to be lost.

In term of SISR tasks, the general goal is to find the mapping function F to maximize the mutual information between HR and SR image.

$$F(I_{LR}; \theta) = I_{SR}; \max_{\theta} I(I_{HR}; F(I_{LR}; \theta)) \quad (2)$$

3.2. Spatial Information Vanish in Super-resolution

Generally speaking, SISR methods [5–7, 21, 24, 50, 57, 58] can generally divided into three parts: (1) shallow feature extraction, (2) deep feature extraction, (3) image reconstruction.

In these methods, there is almost no difference between shallow feature extraction and image reconstruction. The former is composed of simple convolutional layers, while the latter consists of convolutional layers and upsampling layers. However, deep feature extraction differs significantly. Yet, their commonality lies in being composed of various residual blocks, which can be simply defined as:

$$X^{l+1} = X^l + f_\theta^{l+1}(X^l) \quad (3)$$

where X indicates inputs, f is a consecutive layers for l ’th residual group, and θ represents the parameters of f^l .

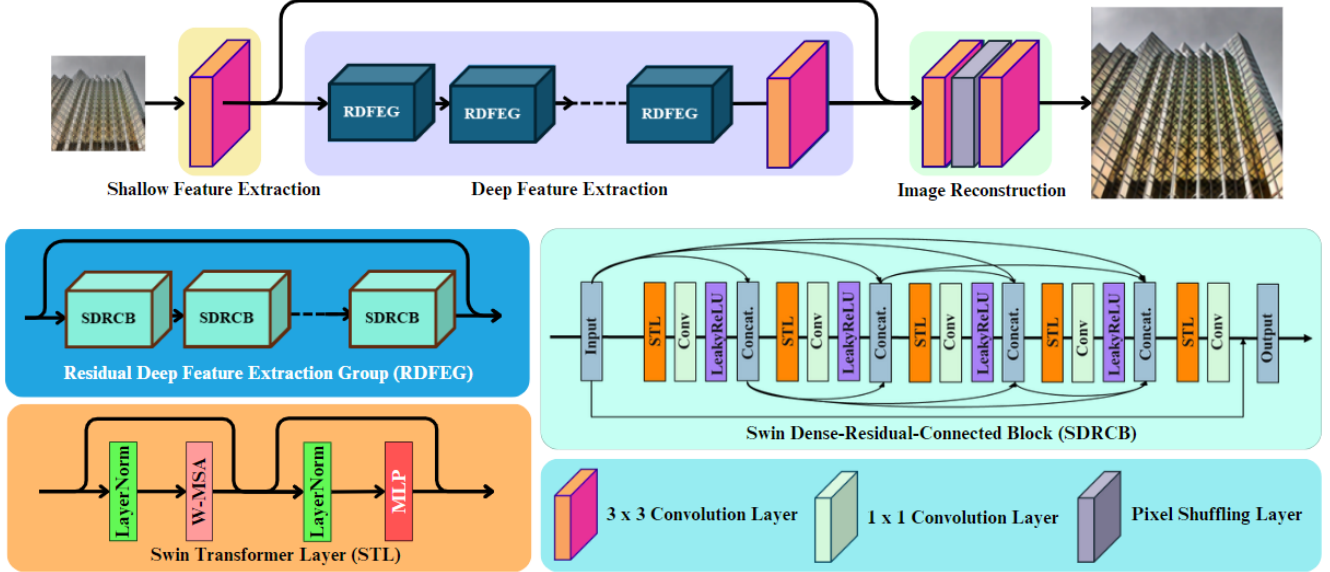


Figure 4. The overall architecture of the proposed DRCT and the structure of RDSEG and SDRCB.

Using residual learning allows the model to only update the differences between layers, rather than predicting the total output of a layer directly. This reduces the difficulty of model training and prevents gradient vanishing. However, according to our observations, while this design effectively transmits spatial information between different residual blocks, there may still be information loss.

Because the information within a residual block may not necessarily maintain spatial information, this ultimately leads to non-smoothness in terms of feature map intensity (refer to Fig. 2 and 3), causing an information bottleneck at the deepest layers during forward propagation. This makes it easy for spatial information to be lost as the gradient flow reaches the deeper layers of the network, resulting in reduced data efficiency or the need for more complex network designs to achieve better performance.

To better evaluate information loss, the G-index is defined by the sum of two components: the absolute change in the maximum intensities and the absolute change in the minimum intensities of the feature maps. It quantifies the absolute difference in both the highest and lowest feature map intensities between two consecutive layers.

$$GI = \sum_{l=1}^L (\|\Delta G_{min}^l\| + \|\Delta G_{max}^l\|) \quad (4)$$

where L is the depth of network. G-index, encapsulating the total of these absolute changes, acts as a measure directly proportional to the information loss within the network. (refer to Figure 3.)

3.3. Dense-Residual Group Auxiliary Supervision

Motivated by RRDB [43], Wang *et al.* suggested that incorporating dense-residual connections can aggregate multi-level feature information and stabilize training through residual learning [25, 34]. Nonetheless, CNN-based approaches, which primarily focus on learning local information, often overlook the importance of capturing long-range dependencies. Recent studies on SwinIR-based methods have concentrated on enlarging the receptive field [5, 6, 58] or enhancing the network's capability to extract features [21, 44].

By adding dense connections within SwinIR-based blocks, we believe that it is possible to stabilize the gradient flow within each residual group during back-propagation, thereby addressing the issue of information bottlenecks and enhancing the receptive field. Consequently, this approach allows for achieving outstanding performance with simpler model architectures, or even by using shallower SISR networks.

4. Methodology

4.1. Network Architecture

As shown in Fig. 4, DRCT is composed of three distinct components: shallow feature extraction, deep feature extraction and image reconstruction module.

Shallow and deep feature extraction Given a low-resolution (LR) input $I_{LR} \in \mathbb{R}^{H \times W \times C_{in}}$ (H , W and C_{in} are the image height, width and input channel number, respectively), we use a 3×3 convolutional layer $\mathcal{C}_3(\cdot)$ [45] to

extract shallow feature $F_0 \in \mathbb{R}^{H \times W \times C}$ as

$$F_0 = \mathcal{C}_3(I_{LQ}), \quad (5)$$

Then, we extract deep feature which contains high-frequency spatial information $F_{DF} \in \mathbb{R}^{H \times W \times C}$ from F_0 and it can be defined as

$$F_{DF} = H_{DF}(F_0), \quad (6)$$

where $H_{DF}(\cdot)$ is the deep feature extraction module and it contains K Residual deep feature extraction group (RDFEG) and a convolutional layer \mathcal{C}_3 . More specifically, intermediate features F_1, F_2, \dots, F_K and the output deep feature F_{DF} are extracted block by block as

$$F_i = RDFEG_i(F_{i-1}), \quad i = 1, 2, \dots, K, \quad (7)$$

$$F_{DF} = \mathcal{C}_3(F_K), \quad (8)$$

Image reconstruction. We reconstruct the SR image $I_{SR} \in \mathbb{R}^{H \times W \times C_{in}}$ by aggregating shallow and deep features, it can be defined as:

$$I_{SR} = H_{REC}(F_0 + F_{DF}), \quad (9)$$

where $H_{REC}(\cdot)$ is the function of the reconstruction module for fusing high-frequency deep feature F_{DF} and low-frequency feature F_0 together to obtain SR result.

4.2. Residual Deep Feature Extraction Group and Swin-Dense-Residual-Connected Block

In developing the RDFEG, we take cues from [16] and [43], employing a residual-dense block (RDB) as the foundational unit. The reuse of feature maps emerges as the enhanced receptive field in the RDB's feed-forward mechanism. The RDFEG contains a Swin-dense-residual-connected block (SDRCB) (refer to Figure 4), and the SDRCB can be defined as:

$$\begin{aligned} X_1 &= PE(\mathcal{C}_\sigma(PUE(STL(X)))) \\ X_2 &= PE(\mathcal{C}_\sigma(PUE(STL(Cat.(X, X_1),)))) \\ X_3 &= PE(\mathcal{C}_\sigma(PUE(STL(Cat.(X, X_1, X_2),)))) \\ X_4 &= PE(\mathcal{C}_\sigma(PUE(STL(Cat.(X, X_1, X_2, X_3),)))) \\ X_5 &= PE(\mathcal{C}_1(PUE(STL(Cat.(X, X_1, X_2, X_3, X_4),)))) \end{aligned}$$

$$SDRCB(X) = \alpha \cdot X_5 + X \quad (10)$$

where $Cat(\cdot)$ denotes the concatenation operator, which is designed to fuse multi-level feature. $STL(\cdot)$ represents the Swin-Transformer layer [24]. $PE(\cdot)$ and $PUE(\cdot)$ are the

patch embedding and patch unembedding operations [11], respectively. \mathcal{C}_σ is the 1×1 convolutional layer with a LeakyReLU activate function for feature transition. The negative slope of LeakyReLU is set to 0.2. \mathcal{C}_1 is the 1×1 convolutional layer. α is set to 0.2 for stabilizing the training process [43].

4.3. Same-task Progressive Training

In recent years, Progressive Training Strategy (PTS) [12, 54] have gained increased attention and can be seen as a method of fine-tuning. Compared to conventional training methods, PTS tends to converge model parameters to more desirable local-minima. Within the field of image processing, IPT [3] employs a variety of low-level tasks for pre-training, while EDT [22] utilizes different degradation levels within a single task. HAT [5] introduces the concept of same-task pre-training, where training on a larger and more diverse dataset like ImageNet [9] before fine-tuning on a specific dataset leads to improved super-resolution results. Lei *et al.* [49] proposed initially training a SISR network with L1-loss and then using L2-loss to eliminate artifacts, achieving better results on the PSNR metric. This concept has been widely adopted [58]. Our proposed Same-task Progressive Training (SPT), we first pre-trained DRCT on ImageNet to initialize model parameters and then fine-tuned on specific dataset with L1 loss as the optimization objective function,

$$\text{Loss}_1 = \|I_{HR} - I_{SR}\|_1 \quad (11)$$

and finally use L2 loss to eliminate singular pixels and artifacts, therefore further archiving greater performance on PSNR metrics.

$$\text{Loss}_2 = \|I_{HR} - I_{SR}\|_2 \quad (12)$$

5. Experiment Results

5.1. Dataset

Our DRCT model is trained on DF2K, a substantial aggregated dataset that includes DIV2K [1] and Flickr2K [36]. DIV2K provides 800 images for training, while Flickr2K contributes a larger set of 2650 images. For the training input, we generate low-resolution versions of these images by applying a bicubic downsampling method with scaling factors of 2, 3, and 4, respectively. To assess the effectiveness of our model, we conduct performance evaluations using well-known Image Super-Resolution benchmark datasets such as Set5 [2], Set14 [48], BSD100 [29], Urban100 [17], and Manga109 [30], which are standard in SISR tasks.

5.2. Implementation Details

The training process can be structured into three distinct phases, as illustrated as Section 4-3. (1) pre-trained on Im-

Method	Scale	Training Dataset	Set5 [2]		Set14 [48]		BSD100 [29]		Urban100 [17]		Manga109 [30]	
			PSNR	SSIM	PSNR	SSIM	PSNR	SSIM	PSNR	SSIM	PSNR	SSIM
EDSR [25]	$\times 2$	DIV2K	38.11	0.9602	33.92	0.9195	32.32	0.9013	32.93	0.9351	39.10	0.9773
RCAN [52]	$\times 2$	DIV2K	38.27	0.9614	34.12	0.9216	32.41	0.9027	33.34	0.9384	39.44	0.9786
SAN [8]	$\times 2$	DIV2K	38.31	0.9620	34.07	0.9213	32.42	0.9028	33.10	0.9370	39.32	0.9792
IGNN [56]	$\times 2$	DIV2K	38.24	0.9613	34.07	0.9217	32.41	0.9025	33.23	0.9383	39.35	0.9786
HAN [32]	$\times 2$	DIV2K	38.27	0.9614	34.16	0.9217	32.41	0.9027	33.35	0.9385	39.46	0.9785
NLSN [31]	$\times 2$	DIV2K	38.34	0.9618	34.08	0.9231	32.43	0.9027	33.42	0.9394	39.59	0.9789
SwinIR [24]	$\times 2$	DF2K	38.42	0.9623	34.46	0.9250	32.53	0.9041	33.81	0.9427	39.92	0.9797
CAT-A [6]	$\times 2$	DF2K	38.51	0.9626	34.78	0.9265	32.59	0.9047	34.26	0.9440	40.10	0.9805
HAT [5]	$\times 2$	DF2K	38.63	0.9630	34.86	0.9274	32.62	0.9053	34.45	0.9466	40.26	0.9809
DAT [7]	$\times 2$	DF2K	38.58	0.9629	34.81	0.9272	32.61	0.9051	34.37	0.9458	40.33	0.9807
DRCT (Ours)	$\times 2$	DF2K	38.80	0.9646	35.02	0.9291	32.79	0.9071	34.58	0.9474	40.41	0.9816
IPT \dagger [3]	$\times 2$	ImageNet	38.37	-	34.43	-	32.48	-	33.76	-	-	-
EDT \dagger [22]	$\times 2$	DF2K	38.63	0.9632	34.80	0.9273	32.62	0.9052	34.27	0.9456	40.37	0.9811
HAT-L \dagger [5]	$\times 2$	DF2K	38.91	0.9646	35.29	0.9293	32.74	0.9066	35.09	0.9505	41.01	0.9831
DRCT-L\dagger (Ours)	$\times 2$	DF2K	39.14	0.9658	35.36	0.9302	32.90	0.9078	35.17	0.9516	41.14	0.9842
EDSR [25]	$\times 3$	DIV2K	34.65	0.9280	30.52	0.8462	29.25	0.8093	28.80	0.8653	34.17	0.9476
RCAN [52]	$\times 3$	DIV2K	34.74	0.9299	30.65	0.8482	29.32	0.8111	29.09	0.8702	34.44	0.9499
SAN [8]	$\times 3$	DIV2K	34.75	0.9300	30.59	0.8476	29.33	0.8112	28.93	0.8671	34.30	0.9494
IGNN [56]	$\times 3$	DIV2K	34.72	0.9298	30.66	0.8484	29.31	0.8105	29.03	0.8696	34.39	0.9496
HAN [32]	$\times 3$	DIV2K	34.75	0.9299	30.67	0.8483	29.32	0.8110	29.10	0.8705	34.48	0.9500
NLSN [31]	$\times 3$	DIV2K	34.85	0.9306	30.70	0.8485	29.34	0.8117	29.25	0.8726	34.57	0.9508
SwinIR [24]	$\times 3$	DF2K	34.97	0.9318	30.93	0.8534	29.46	0.8145	29.75	0.8826	35.12	0.9537
CAT-A [6]	$\times 3$	DF2K	35.06	0.9326	31.04	0.8538	29.52	0.8160	30.12	0.8862	35.38	0.9546
HAT [5]	$\times 3$	DF2K	35.07	0.9329	31.08	0.8555	29.54	0.8167	30.23	0.8896	35.53	0.9552
DAT [7]	$\times 3$	DF2K	35.16	0.9331	31.11	0.8550	29.55	0.8169	30.18	0.8886	35.59	0.9554
DRCT (Ours)	$\times 3$	DF2K	35.18	0.9338	31.24	0.8569	29.68	0.8182	30.34	0.8910	35.76	0.9575
IPT \dagger [3]	$\times 3$	ImageNet	34.87	-	30.85	-	29.38	-	29.49	-	-	-
EDT \dagger [22]	$\times 3$	DF2K	35.13	0.9328	31.09	0.8553	29.53	0.8165	30.07	0.8863	35.47	0.9550
HAT-L \dagger [5]	$\times 3$	DF2K	35.28	0.9345	31.47	0.8584	29.63	0.8191	30.92	0.8981	36.02	0.9576
DRCT-L\dagger (Ours)	$\times 3$	DF2K	35.32	0.9348	31.54	0.8591	29.68	0.8211	31.14	0.9004	36.16	0.9585
EDSR [25]	$\times 4$	DIV2K	32.46	0.8968	28.80	0.7876	27.71	0.7420	26.64	0.8033	31.02	0.9148
RCAN [52]	$\times 4$	DIV2K	32.63	0.9002	28.87	0.7889	27.77	0.7436	26.82	0.8087	31.22	0.9173
SAN [8]	$\times 4$	DIV2K	32.64	0.9003	28.92	0.7888	27.78	0.7436	26.79	0.8068	31.18	0.9169
IGNN [56]	$\times 4$	DIV2K	32.57	0.8998	28.85	0.7891	27.77	0.7434	26.84	0.8090	31.28	0.9182
HAN [32]	$\times 4$	DIV2K	32.64	0.9002	28.90	0.7890	27.80	0.7442	26.85	0.8094	31.42	0.9177
NLSN [31]	$\times 4$	DIV2K	32.59	0.9000	28.87	0.7891	27.78	0.7444	26.96	0.8109	31.27	0.9184
SwinIR [24]	$\times 4$	DF2K	32.92	0.9044	29.09	0.7950	27.92	0.7489	27.45	0.8254	32.03	0.9260
CAT-A [6]	$\times 4$	DF2K	33.08	0.9052	29.18	0.7960	27.99	0.7510	27.89	0.8339	32.39	0.9285
HAT [5]	$\times 4$	DF2K	33.04	0.9056	29.23	0.7973	28.00	0.7517	27.97	0.8368	32.48	0.9292
DAT [7]	$\times 4$	DF2K	33.08	0.9055	29.23	0.7973	28.00	0.7515	27.87	0.8343	32.51	0.9291
DRCT (Ours)	$\times 4$	DF2K	33.11	0.9064	29.35	0.7984	28.18	0.7532	28.06	0.8378	32.59	0.9304
IPT \dagger [3]	$\times 4$	ImageNet	32.64	-	29.01	-	27.82	-	27.26	-	-	-
EDT [22]	$\times 4$	DF2K	32.82	0.9031	29.09	0.7939	27.91	0.7483	27.46	0.8246	32.05	0.9254
HAT-L \dagger [5]	$\times 4$	DF2K	33.30	0.9083	29.47	0.8015	28.09	0.7551	28.60	0.8498	33.09	0.9335
DRCT-L\dagger (Ours)	$\times 4$	DF2K	33.37	0.9090	29.54	0.8025	28.16	0.7577	28.70	0.8508	33.14	0.9347

Table 1. Quantitative comparison with the several peer-methods on benchmark datasets. “ \dagger ” indicates that methods adopt pre-training strategy [5] on ImageNet. “ \ddagger ” represents that methods use same-task progressive-training strategy. The top three results are marked in **red**, **blue**, and **orange**, respectively.

ageNet [9], (2) optimize the model on the given dataset, (3) L2-loss for PSNR enhancement. Throughout the training process, we use the Adam optimizer with $\beta_1 = 0.9$, and $\beta_2 = 0.999$ and train for $800k$ iterations in each stage. The

learning rate is set to $2e - 4$, the multi-step learning scheduler is also used. The learning rate is halved at the $300k$, $500k$, $650k$, $700k$, $750k$ iterations respectively. Weight decay is not applied and the batch-size is set to 32. In the ar-

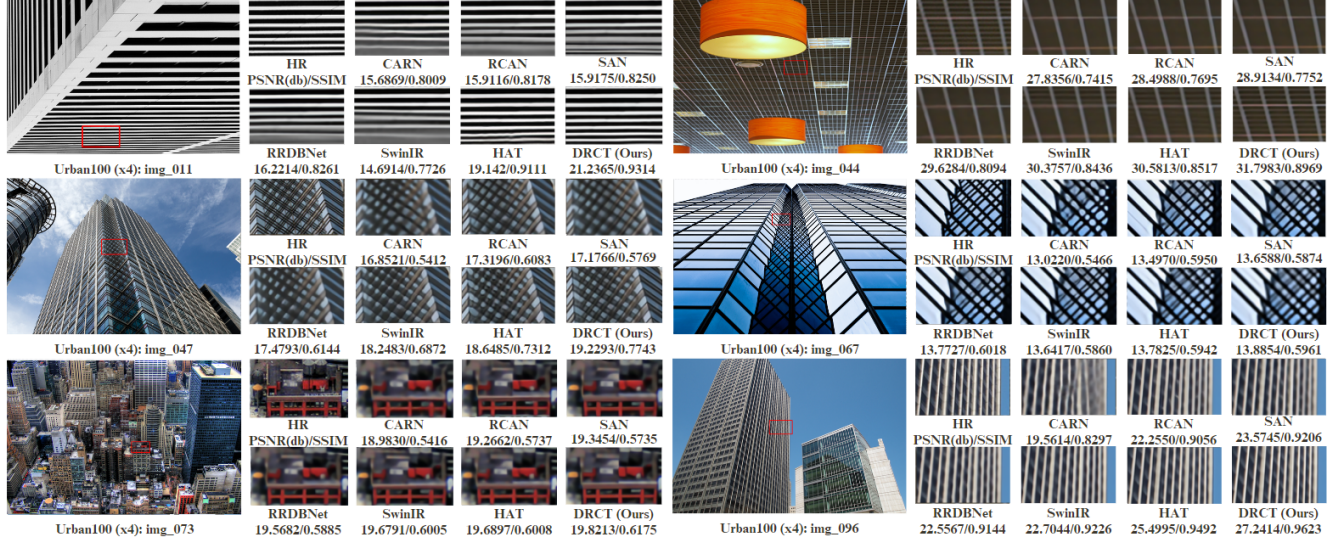


Figure 5. Visual comparison on $\times 4$ SISR. The patches for comparison are marked with red boxes in the original images. The higher the PSNR/SSIM metrics, the better the performance..

chitecture of DRCT, the configuration of depth and width is maintained identically to that of SwinIR. To elaborate, both the number of RDSEG and SDRCB units are established at 6, and the channel number of intermediate feature maps is designated as 180. The attention head number and window size are set to 6 and 16 for window-based multi head self-attention (W-MSA). In terms of data preparation, HR patches with dimensions of 256×256 pixels were extracted from the HR images. To improve the generalizability, we apply random horizontal flips and rotation augmentation.

5.3. Quantitative Results

For the evaluation, we use full RGB channels and ignore the $(2 \times \text{scale})$ pixels from the border. PSNR and SSIM metrics are used to evaluation criteria. Table 1 presents the quantitative comparison of our approach and the state-of-the-art methods, including EDSR [25], RCAN [52], SAN [8], IGN [56], HAN [32], NLSN [31], SwinIR [24], CAT-A [6], DAT [7], as well as approaches using ImageNet pre-training, such as IPT [3], EDT [22] and HAT [5]. We can see that our method outperforms the other methods significantly on all benchmark datasets. In addition, the DRCT-L can bring further improvement and greatly expands the performance upper-bound of this task. Even with fewer model parameters and computational requirements, DRCT is also significantly greater than the state-of-the-art methods.

5.4. Visual Comparison

The visual comparisons displayed in Figure 5. For the selected images from the Urban100 [17], DRCT is effective in restoring structures, whereas other methods suffer from notably blurry effects. The visual results demonstrate the

superiority of our approach.

Along with providing visualizations for the LAM [13], we compute the DI and GI. In scenarios where DRCT operates with fewer parameters (a topic for the next subsection), it achieves a higher DI. This outcome suggests that, after enhancing the receptive field through SDRCB, the model can leverage a greater amount of non-local information for SISR without the need for intricately designed W-MSA. Additionally, the GI of the proposed DRCT, being the lowest among the three, underscores its training process stability and its effectiveness in minimizing information loss.

There remains significant room for improvement in the way information loss is measured for SISR models. We conducted a detailed analysis of the G-index using 'image_092' from Urban100, as shown in Figure 6. DRCT managed to achieve a lower score on the GI, indicating that the changes in the network's feature maps are relatively stable. In contrast, The GI for HAT was significantly higher than the other two, which suggests that a lower GI value can effectively denote lesser information loss, whereas a higher GI might imply more drastic changes in feature maps. However, this doesn't necessarily correlate directly with the effectiveness of measuring information loss.

5.5. Model Complexity

To demonstrate the potential of our proposed method, we conducted further analysis on model complexity, with the results illustrated in Figure 7. From the figure, we can observe that the performance curves of the HAT and SwinIR models are approaching horizontal lines, suggesting that their model performance is nearing a bottleneck. Enhancing performance may require significantly more complex mod-

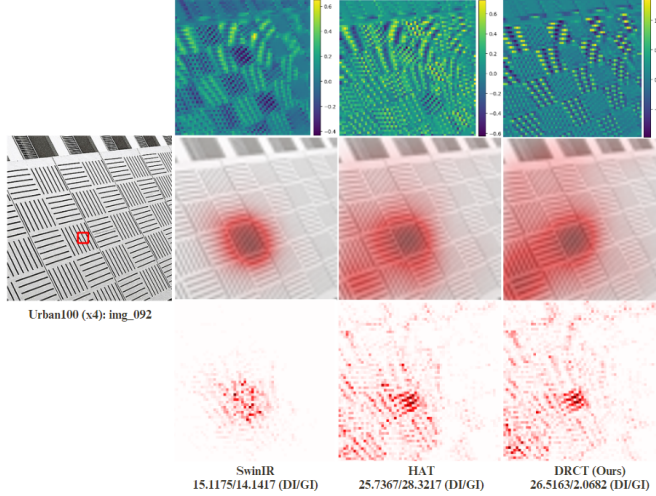


Figure 6. The LAM [13] visualization. DRCT improves performance by enhancing the receptive field to mitigate the issue of spatial information loss in deeper layers of the network. (zoom in to better see the color-bar of feature maps.)

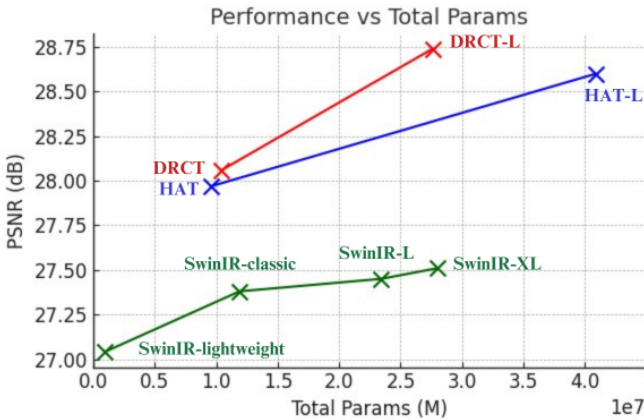


Figure 7. The model complexity comparison between SwinIR, HAT, and proposed DRCT evaluated on Urban100 [17] dataset.

els or a greater number of parameters, potentially leading to prohibitive costs and practical implementation challenges. In contrast, our DRCT-L model outperforms HAT-L while saving 33% of model parameters. This indicates that stabilizing the training and inference processes within residual blocks through a dense-group is a viable strategy to prevent SISR models from encountering information bottlenecks.

5.6. NTIRE Image Super-Resolution (x4) Challenge

The dataset for the NTIRE 2024 Image Super-Resolution (x4) Challenge comprises three collections: DIV2K [1], Flickr2K [36], and LSDIR [23]. Specifically, the DIV2K dataset provides 800 pairs of high and low-resolution images for training. For validation, it offers 100 low-resolution

	Validation phase	Testing phase
PSNR	31.4852	31.7784
SSIM	0.8563	0.8655

Table 2. NTIRE 2024 Challenge Results with x4 SR in terms of PSNR and SSIM on validation phase and testing phase.

images for the purpose of creating super-resolution counterparts, with the high-resolution versions to be made available at the challenge’s final stage. Additionally, the test dataset includes 100 varied images for generating their low-resolution equivalents. A self-ensemble strategy is used for testing-time augmentation (TTA) [35]. Our TTA methods include rotation, and horizontal and vertical flipping. We also conduct a model ensemble for fusing different reconstructed results by HAT [5] and the proposed DRCT. Our super-resolution (SR) model was entered into both the validation and testing phases of this Challenge, with the outcomes detailed in Table 2.

6. Conclusion

In this paper, we introduce the phenomenon of information bottlenecks observed in SISR models, where spatial information is lost as network depth increases during the forward-propagation process. This may lead to gradient vanishing and severe oscillations in the distribution of feature intensities, limiting the upper bound of model performance for the SISR task.

To address this issue, we present a novel Swin-transformer-based model named the Dense-residual-connected Transformer (DRCT). The design philosophy behind DRCT centers on stabilizing the forward-propagation process and enhancing the receptive field by incorporating dense connections within residual blocks. This approach reduces the loss of spatial information, addressing the information bottleneck issues that SISR models may encounter in deeper network layers.

As a result, the model can better focus on global spatial information and surpass existing state-of-the-art methods without the need for designing complex window attention mechanisms or increasing model parameters.

The extensive experiments demonstrate that DRCT surpasses previous methods in image super-resolution, indicating its effectiveness and the benefits of the proposed approach.

References

- [1] Eirikur Agustsson and Radu Timofte. Ntire 2017 challenge on single image super-resolution: Dataset and study. In *The IEEE Conference on Computer Vision and Pattern Recognition (CVPR) Workshops*, 2017. 5, 8

[2] Marco Bevilacqua, Aline Roumy, Christine Guillemot, and Marie Line Alberi-Morel. Low-complexity single-image super-resolution based on nonnegative neighbor embedding. 2012. 5, 6

[3] Hanting Chen, Yunhe Wang, Tianyu Guo, Chang Xu, Yiping Deng, Zhenhua Liu, Siwei Ma, Chunjing Xu, Chao Xu, and Wen Gao. Pre-trained image processing transformer, 2021. 1, 2, 5, 6, 7

[4] Qiang Chen, Qiman Wu, Jian Wang, Qinghao Hu, Tao Hu, Errui Ding, Jian Cheng, and Jingdong Wang. Mixformer: Mixing features across windows and dimensions, 2022. 2

[5] Xiangyu Chen, Xintao Wang, Jiantao Zhou, Yu Qiao, and Chao Dong. Activating more pixels in image super-resolution transformer, 2023. 2, 3, 4, 5, 6, 7, 8

[6] Zheng Chen, Yulun Zhang, Jinjin Gu, Yongbing Zhang, Linghe Kong, and Xin Yuan. Cross aggregation transformer for image restoration. In *NeurIPS*, 2022. 2, 4, 6, 7

[7] Zheng Chen, Yulun Zhang, Jinjin Gu, Linghe Kong, Xiaokang Yang, and Fisher Yu. Dual aggregation transformer for image super-resolution. In *ICCV*, 2023. 2, 3, 6, 7

[8] Tao Dai, Jianrui Cai, Yongbing Zhang, Shu-Tao Xia, and Lei Zhang. Second-order attention network for single image super-resolution. In *Proceedings of the IEEE Conference on Computer Vision and Pattern Recognition*, pages 11065–11074, 2019. 1, 6, 7

[9] Jia Deng, Wei Dong, Richard Socher, Li-Jia Li, Kai Li, and Li Fei-Fei. Imagenet: A large-scale hierarchical image database. In *2009 IEEE Conference on Computer Vision and Pattern Recognition*, pages 248–255, 2009. 1, 5, 6

[10] Chao Dong, Chen Change Loy, Kaiming He, and Xiaoou Tang. Image super-resolution using deep convolutional networks, 2015. 1

[11] Alexey Dosovitskiy et al. An image is worth 16x16 words: Transformers for image recognition at scale, 2021. 2, 5

[12] Keyao Wang et al. Dynamic feature queue for surveillance face anti-spoofing via progressive training. In *Proceedings of the IEEE/CVF Conference on Computer Vision and Pattern Recognition (CVPR)*, 2023. 5

[13] Jinjin Gu and Chao Dong. Interpreting super-resolution networks with local attribution maps. In *Proceedings of the IEEE/CVF Conference on Computer Vision and Pattern Recognition*, pages 9199–9208, 2021. 7, 8

[14] Chaoxu Guo, Bin Fan, Qian Zhang, Shiming Xiang, and Chunhong Pan. Augfpn: Improving multi-scale feature learning for object detection, 2019. 2

[15] Zeeshan Hayder, Xuming He, and Mathieu Salzmann. Boundary-aware instance segmentation, 2017. 2

[16] Chih-Chung Hsu, Chih-Yu Jian, Eng-Shen Tu, Chia-Ming Lee, and Guan-Lin Chen. Real-time compressed sensing for joint hyperspectral image transmission and restoration for cubesat. *IEEE Transactions on Geoscience and Remote Sensing*, pages 1–1, 2024. 2, 5

[17] Jia-Bin Huang, Abhishek Singh, and Narendra Ahuja. Single image super-resolution from transformed self-exemplars. In *Proceedings of the IEEE Conference on Computer Vision and Pattern Recognition*, pages 5197–5206, 2015. 5, 6, 7, 8

[18] Kuan-Chih Huang, Tsung-Han Wu, Hung-Ting Su, and Winston H. Hsu. Monodtr: Monocular 3d object detection with depth-aware transformer, 2022. 2

[19] Christian Ledig, Lucas Theis, Ferenc Huszar, Jose Caballero, Andrew Cunningham, Alejandro Acosta, Andrew Aitken, Alykhan Tejani, Johannes Totz, Zehan Wang, and Wenzhe Shi. Photo-realistic single image super-resolution using a generative adversarial network, 2017. 1

[20] Chen-Yu Lee, Saining Xie, Patrick Gallagher, Zhengyou Zhang, and Zhuowen Tu. Deeply-Supervised Nets. In *Proceedings of the Eighteenth International Conference on Artificial Intelligence and Statistics*, pages 562–570, San Diego, California, USA, 2015. PMLR. 2

[21] Ao Li, Le Zhang, Yun Liu, and Ce Zhu. Feature modulation transformer: Cross-refinement of global representation via high-frequency prior for image super-resolution. In *Proceedings of the IEEE/CVF International Conference on Computer Vision*, pages 12514–12524, 2023. 2, 3, 4

[22] Wenbo Li, Xin Lu, Shengju Qian, Jiangbo Lu, Xiangyu Zhang, and Jiaya Jia. On efficient transformer and image pre-training for low-level vision. *arXiv preprint arXiv:2112.10175*, 2021. 1, 5, 6, 7

[23] Yawei et al. Li. Lsdir: A large scale dataset for image restoration. In *Proceedings of the IEEE/CVF Conference on Computer Vision and Pattern Recognition (CVPR) Workshops*, pages 1775–1787, 2023. 8

[24] Jingyun Liang, Jiezhang Cao, Guolei Sun, Kai Zhang, Luc Van Gool, and Radu Timofte. Swinir: Image restoration using swin transformer. *arXiv preprint arXiv:2108.10257*, 2021. 1, 2, 3, 5, 6, 7

[25] Bee Lim, Sanghyun Son, Heewon Kim, Seungjun Nah, and Kyoung Mu Lee. Enhanced deep residual networks for single image super-resolution. In *The IEEE Conference on Computer Vision and Pattern Recognition (CVPR) Workshops*, 2017. 1, 4, 6, 7

[26] Jie Liu, Wenjie Zhang, Yuting Tang, Jie Tang, and Gangshan Wu. Residual feature aggregation network for image super-resolution. In *2020 IEEE/CVF Conference on Computer Vision and Pattern Recognition (CVPR)*, pages 2356–2365, 2020. 1, 2

[27] Ze Liu, Yutong Lin, Yue Cao, Han Hu, Yixuan Wei, Zheng Zhang, Stephen Lin, and Baining Guo. Swin transformer: Hierarchical vision transformer using shifted windows, 2021. 1, 2

[28] Jiayi Ma, Linfeng Tang, Fan Fan, Jun Huang, Xiaoguang Mei, and Yong Ma. Swinfusion: Cross-domain long-range learning for general image fusion via swin transformer. *IEEE/CAA Journal of Automatica Sinica*, 9(7):1200–1217, 2022. 2

[29] D. Martin, C. Fowlkes, D. Tal, and J. Malik. A database of human segmented natural images and its application to evaluating segmentation algorithms and measuring ecological statistics. In *Proceedings Eighth IEEE International Conference on Computer Vision. ICCV 2001*, pages 416–423 vol.2, 2001. 5, 6

[30] Yusuke Matsui, Kota Ito, Yuji Aramaki, Azuma Fujimoto, Toru Ogawa, Toshihiko Yamasaki, and Kiyoharu Aizawa.

Sketch-based manga retrieval using manga109 dataset. *Multimedia Tools and Applications*, 76(20):21811–21838, 2017. 5, 6

[31] Yiqun Mei, Yuchen Fan, and Yuqian Zhou. Image super-resolution with non-local sparse attention. In *Proceedings of the IEEE/CVF Conference on Computer Vision and Pattern Recognition (CVPR)*, pages 3517–3526, 2021. 1, 6, 7

[32] Ben Niu, Weilei Wen, Wenqi Ren, Xiangde Zhang, Lianping Yang, Shuzhen Wang, Kaihao Zhang, Xiaochun Cao, and Haifeng Shen. Single image super-resolution via a holistic attention network, 2020. 1, 6, 7

[33] Christian Szegedy, Wei Liu, Yangqing Jia, Pierre Sermanet, Scott Reed, Dragomir Anguelov, Dumitru Erhan, Vincent Vanhoucke, and Andrew Rabinovich. Going deeper with convolutions, 2014. 2

[34] Christian Szegedy, Sergey Ioffe, Vincent Vanhoucke, and Alex Alemi. Inception-v4, inception-resnet and the impact of residual connections on learning, 2016. 4

[35] Radu Timofte, Rasmus Rothe, and Luc Van Gool. Seven ways to improve example-based single image super resolution, 2015. 8

[36] Radu Timofte, Eirikur Agustsson, Luc Van Gool, Ming-Hsuan Yang, Lei Zhang, Bee Lim, et al. Ntire 2017 challenge on single image super-resolution: Methods and results. In *The IEEE Conference on Computer Vision and Pattern Recognition (CVPR) Workshops*, 2017. 5, 8

[37] Naftali Tishby and Noga Zaslavsky. Deep learning and the information bottleneck principle. In *2015 IEEE Information Theory Workshop (ITW)*, pages 1–5, 2015. 2

[38] Tong Tong, Gen Li, Xiejie Liu, and Qinquan Gao. Image super-resolution using dense skip connections. In *2017 IEEE International Conference on Computer Vision (ICCV)*, pages 4809–4817, 2017. 1

[39] Chien-Yao Wang and Hong-Yuan Mark Liao. YOLOv9: Learning what you want to learn using programmable gradient information. 2024. 2

[40] Chien-Yao Wang, Hong-Yuan Mark Liao, I-Hau Yeh, Yueh-Hua Wu, Ping-Yang Chen, and Jun-Wei Hsieh. CspNet: A new backbone that can enhance learning capability of cnn, 2019. 2

[41] Chien-Yao Wang, Hong-Yuan Mark Liao, and I-Hau Yeh. Designing network design strategies through gradient path analysis. *arXiv preprint arXiv:2211.04800*, 2022. 2

[42] Chien-Yao Wang, Alexey Bochkovskiy, and Hong-Yuan Mark Liao. Yolov7: Trainable bag-of-freebies sets new state-of-the-art for real-time object detectors. In *Proceedings of the IEEE/CVF Conference on Computer Vision and Pattern Recognition (CVPR)*, pages 7464–7475, 2023. 2

[43] Xintao Wang, Ke Yu, Shixiang Wu, Jinjin Gu, Yihao Liu, Chao Dong, Yu Qiao, and Chen Change Loy. Esrgan: Enhanced super-resolution generative adversarial networks. In *The European Conference on Computer Vision Workshops (ECCVW)*, 2018. 1, 2, 4, 5

[44] Zhendong Wang, Xiaodong Cun, Jianmin Bao, Wengang Zhou, Jianzhuang Liu, and Houqiang Li. Uformer: A general u-shaped transformer for image restoration, 2021. 2, 4

[45] Tete Xiao, Mannat Singh, Eric Mintun, Trevor Darrell, Piotr Dollár, and Ross Girshick. Early convolutions help transformers see better, 2021. 4

[46] Yue Yang and Yong Qi. Image super-resolution via channel attention and spatial graph convolutional network. *Pattern Recognition*, 112:107798, 2021. 1

[47] Syed Waqas Zamir, Aditya Arora, Salman Khan, Munawar Hayat, Fahad Shahbaz Khan, and Ming-Hsuan Yang. Restormer: Efficient transformer for high-resolution image restoration. In *CVPR*, 2022. 2

[48] Roman Zeyde, Michael Elad, and Matan Protter. On single image scale-up using sparse-representations. In *Curves and Surfaces*, pages 711–730, Berlin, Heidelberg, 2012. Springer Berlin Heidelberg. 5, 6

[49] Lei Zha, Yu Yang, Zicheng Lai, Ziwei Zhang, and Juan Wen. A lightweight dense connected approach with attention on single image super-resolution. *Electronics*, 10:1234, 2021. 5

[50] Dafeng Zhang, Feiyu Huang, Shizhuo Liu, Xiaobing Wang, and Zhezhu Jin. Swinfir: Revisiting the swinir with fast fourier convolution and improved training for image super-resolution, 2023. 2, 3

[51] Xindong Zhang, Hui Zeng, Shi Guo, and Lei Zhang. Efficient long-range attention network for image super-resolution, 2022. 2

[52] Yulun Zhang, Kunpeng Li, Kai Li, Lichen Wang, Bineng Zhong, and Yun Fu. Image super-resolution using very deep residual channel attention networks. In *ECCV*, 2018. 1, 6, 7

[53] Yulun Zhang, Yapeng Tian, Yu Kong, Bineng Zhong, and Yun Fu. Residual dense network for image super-resolution. In *2018 IEEE/CVF Conference on Computer Vision and Pattern Recognition*, pages 2472–2481, 2018. 1, 2

[54] Yulun et al. Zhang. Ntire 2023 challenge on image super-resolution (x4): Methods and results. In *2023 IEEE/CVF Conference on Computer Vision and Pattern Recognition Workshops (CVPRW)*, pages 1865–1884, 2023. 5

[55] Daquan Zhou, Zhiding Yu, Enze Xie, Chaowei Xiao, Anima Anandkumar, Jiashi Feng, and Jose M. Alvarez. Understanding the robustness in vision transformers, 2022. 2

[56] Shangchen Zhou, Jiawei Zhang, Wangmeng Zuo, and Chen Change Loy. Cross-scale internal graph neural network for image super-resolution. In *Advances in Neural Information Processing Systems*, 2020. 1, 6, 7

[57] Yupeng Zhou, Zhen Li, Chun-Le Guo, Song Bai, Ming-Ming Cheng, and Qibin Hou. Srformer: Permuted self-attention for single image super-resolution. *arXiv preprint arXiv:2303.09735*, 2023. 2, 3

[58] Qiang Zhu, Pengfei Li, and Qianhui Li. Attention retractable frequency fusion transformer for image super resolution. In *2023 IEEE/CVF Conference on Computer Vision and Pattern Recognition Workshops (CVPRW)*, pages 1756–1763, 2023. 2, 3, 4, 5